The International Journal of Cardiovascular Imaging (2019) 35:1733–1743
https://doi.org/10.1007/s10554-019-01618-5

ORIGINAL PAPER

Hemodynamic impact of coronary stenosis using computed tomography: comparison between noninvasive fractional flow reserve and 3D fusion of coronary angiography with stress myocardial perfusion

Amit R. Patel[1] · Francesco Maffessanti[1,2] · Mita B. Patel[1] · Kalie Kebed[1] · Akhil Narang[1] · Amita Singh[1] · Diego Medvedofsky[1] · S. Javed Zaidi[1,3] · Anuj Mediratta[1] · Neha Goyal[1] · Nadjia Kachenoura[4] · Roberto M. Lang[1] · Victor Mor-Avi[1]

Received: 8 February 2019 / Accepted: 30 April 2019 / Published online: 9 May 2019

Abstract

Vasodilator-stress CT perfusion imaging in addition to CT coronary angiography (CTCA) may provide a single-test alternative to nuclear stress testing, commonly used to assess hemodynamic significance of stenosis. Another alternative is fractional flow reserve (FFR) calculated from cardiac CT images. We studied the concordance between these two approaches and their relationship to outcomes. We prospectively studied 150 patients with chest pain, who underwent CTCA and regadenoson CT. CTCA images were interpreted for presence and severity of stenosis. Fused 3D displays of subendocardial X-ray attenuation with coronary arteries were created to detect stress perfusion defects (SPD) in each coronary territory. In patients with stenosis > 25%, CT-FFR was quantified. Significant stenosis was determined by: (1) combination of stenosis > 50% with an SPD, (2) CT-FFR ≤ 0.80. Patients were followed-up for 36 ± 25 months for death, myocardial infarction or revascularization. After excluding patients with normal arteries and technical/quality issues, in final analysis of 76 patients, CTCA depicted stenosis > 70% in 13/224 arteries, 50–70% in 24, and < 50% in 187. CT-FFR ≤ 0.80 was found in 41/224 arteries, and combination of SPD with > 50% stenosis in 31/224 arteries. Inter-technique agreement was 89%. Despite high incidence of abnormal CT-FFR (30/76 patients), only 7 patients experienced adverse outcomes; 6/7 also had SPDs. Only 1/9 patients with CT-FFR ≤ 0.80 but normal perfusion had an event. Fusion of CTCA and stress perfusion can help determine the hemodynamic impact of stenosis in one test, in good agreement with CT-FFR. Adding stress CT perfusion analysis may help risk-stratify patients with abnormal CT-FFR.

Keywords Fusion imaging · Cardiovascular CT · Vasodilator stress · Myocardial perfusion

Abbreviations

CT	Computed tomography
CTCA	Computed tomography coronary angiography
CTP	Computed tomography perfusion
FFR	Fractional flow reserve
HU	Hounsfeld units
LAD	Left anterior descending
LCX	Left circumflex
LV	Left ventricular
MPI	Myocardial perfusion imaging
RCA	Right coronary artery
SPD	Stress-induced perfusion defect

Electronic supplementary material The online version of this article (https://doi.org/10.1007/s10554-019-01618-5) contains supplementary material, which is available to authorized users.

✉ Victor Mor-Avi
vmoravi@bsd.uchicago.edu

[1] Department of Medicine, Section of Cardiology, University of Chicago Medical Center, 5758 South Maryland Avenue, M.C. 9067, Chicago, IL 60637, USA

[2] Institute of Computational Sciences, Università della Svizzera Italiana, Lugano, Switzerland

[3] Cardiology Department, Advocate Children's Hospital, Chicago, IL, USA

[4] Laboratoire d'Imagerie Biomédicale, INSERM, CNRS, Sorbonne Université, Paris, France

Introduction

Combined assessment of coronary anatomy, i.e. presence and severity of stenosis, and its hemodynamic significance, namely extent of ischemia, is of great clinical importance, especially in patients with chest pain. This is frequently achieved by radionuclide myocardial perfusion imaging triggered by abnormal CT coronary angiography (CTCA), especially in patients with intermediate grade stenosis [1–3]. This is because CTCA is known to overestimate stenosis and because the extent of myocardial ischemia is more important than the severity of stenosis for identifying patients who would benefit from revascularization [4, 5].

A recent alternative to nuclear perfusion imaging is vasodilator CT, designed to detect stress-induced perfusion defects (SPDs), thereby offering the advantage of noninvasive assessment of abnormalities in coronary anatomy and their hemodynamic impact in a single test [6–8]. Although CT perfusion (CTP) imaging has been tested and validated [9–14], it relies on visual assessment of multiple 2D slices, rather than 3D analysis of the entire myocardium, and requires manual adjustment of contrast windows, both carrying the risk of missing small subendocardial perfusion defects. Accordingly, we recently developed fusion software that creates combined 3D displays of the coronary arteries with color maps of myocardial perfusion [15], geared towards combined assessment of the severity of stenosis in each coronary artery and the extent of ischemia it causes in the underlying myocardium.

Furthermore, alternative approaches that do not involve stress and/or additional radiation, may have important implications for greater patient safety and significant cost savings. One such approach, designed to provide information on hemodynamic significance of coronary stenosis is the noninvasive fractional flow reserve (FFR) calculated from resting cardiac CT images using fluid dynamics (CT-FFR) [16–22]. This approach has been validated and is rapidly expanding into clinical practice [23, 24], since its approval for clinical use.

Although stress CTP imaging and CT-FFR both provide information on hemodynamic significance of coronary stenosis, they reflect different aspects of the disease. CT-FFR estimates flow reserve along the artery, similar to invasive coronary FFR measurements obtained from pressure gradients across the stenotic lesion at rest and during stress, which is the current standard used to guide interventions. In contrast, stress CTP reflects the presence and extent of ischemia within the myocardial tissue, rather than at the vessel level, and is thus affected in addition by microvascular dysfunction [25, 26]. The agreement between these two techniques in their determination which stenotic lesion is hemodynamically significant, is not well established. This study was designed to investigate the concordance between stress CTP and CT-FFR in patients with chest pain who are commonly referred for cardiac CT, and to identify the main sources of discordance. Our secondary goal was to determine the relationship between positive findings on CT-FFR and CTP analysis and outcomes in this patient population.

Methods

Study design

This was a prospective study in which we enrolled patients with chest pain referred for CTCA. Figure 1 shows a diagram of the study design. Resting CT images were used for conventional detection of coronary stenosis. Images obtained in patients with stenosis > 25% in at least one artery were analyzed to obtain CT-FFR. Resting images were also used to extract the coronary tree and the 3D endocardial surface for fusion. Vasodilator stress CT images were used to obtain perfusion data, which were mapped onto the 3D surface and fused with the coronary tree. These fused displays were used to detect SPDs in the territory of each artery. Hemodynamically significant disease was determined using two criteria in parallel: (1) a combination of stenosis > 50% on CTCA concomitant with an SPD, reflecting together the anatomical severity and the hemodynamic impact of stenosis [27], and (2) abnormal CT-FFR. These determinations were compared between them on an artery basis. In addition, patients were

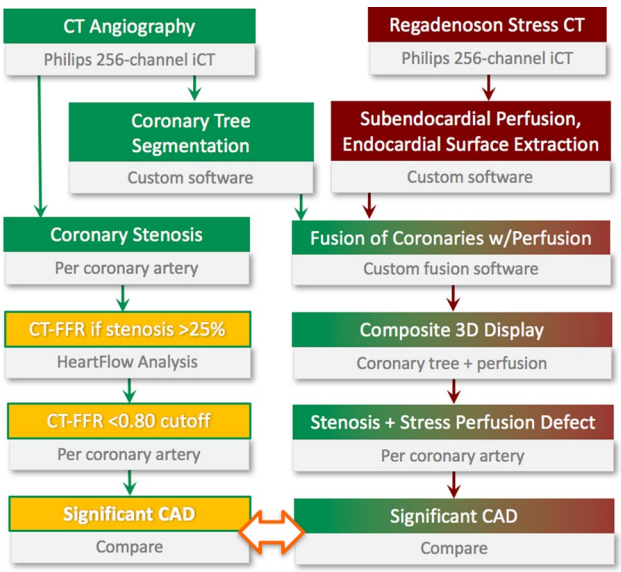

Fig. 1 Schematic diagram of the study design (see text for details)

followed-up for at least 1 year for death, myocardial infarction or revascularization, in order to determine the extent to which the above two criteria are associated with outcomes. To avoid affecting the outcomes, neither CT-FFR nor CTP data were made available to the treating physicians.

Population

We prospectively enrolled 150 patients with chest pain referred for CTCA (age: 55 ± 11 years, 72 males; 48 with hypertension, 16 diabetes mellitus, 56 dyslipidemia; 32 history of tobacco use), who agreed to undergo vasodilator stress CT immediately after, in the same setting. Patients with relative contraindications to CTCA, including known allergies to iodine, renal dysfunction (creatinine > 1.6 mg/dL), inability to perform a 10-s breath-hold, and contraindications to beta-blockers or vasodilators, such as chronic obstructive pulmonary disease, advanced heart block or systolic blood pressure < 90 mmHg, were excluded. This included 28 patients reported in our pilot study [15].

The study was approved by the Institutional Review Board, and each patient signed an informed consent. None of the findings of our research study were conveyed to the physicians who referred the patients for the cardiac CT examinations or the treating physicians. All patients underwent the appropriate clinical management in accordance with their individual needs.

CT imaging

Patients received beta-blocker metoprolol orally (50–100 mg, 1 h prior to imaging) and/or intravenously (5–15 mg immediately prior to imaging), as necessary to achieve a target heart rate of < 65 bpm. Sublingual nitroglycerin (0.4–0.8 mg) was administered, provided that systolic blood pressure was > 100 mmHg. Images were acquired during suspended respiration using a 256-channel scanner (Philips iCT). After resting imaging was performed according to a standard clinical CTCA protocol, regadenoson (Astellas, Deerfield IL), was administered (0.4 mg, i.v.) ≥ 15 min later to ensure contrast clearance. An additional set of images was acquired 1 min after regadenoson to ensure peak effect. Retrospective gating at end-systole was used to avoid "slab" artifacts that were found to frequently affect perfusion evaluation with prospective gating [15]. Dose modulation was used to minimize radiation exposure [13], with gantry rotation time 270 ms, slice thickness 0.625 mm, tube currents 600–1000 mA and voltage 100–120 kV (depending on body weight). The resultant effective radiation dose was 5.5 ± 4.6 mSv, including both the resting CT angiography and stress perfusion imaging. Patients received a bolus of iodinated contrast agent (~ 65 ml, 5 ml/s), which was injected into the right antecubital vein and followed by a 20-ml saline bolus. Image acquisition was triggered by the appearance of contrast in the descending thoracic aorta, 5 s after attenuation increased > 50 Hounsfield units.

Stress CTP analysis

Stress CT images were analyzed using previously described custom software for volumetric analysis and display of myocardial perfusion [13, 28, 29]. Briefly, following semi-automated identification of the endo- and epicardial surfaces, the 3D region of interest confined between them was identified as LV myocardium. Coronary arteries and contrast-filled inter-trabecular spaces were excluded from the myocardium and papillary muscles and trabeculae were excluded from the LV cavity by setting thresholds on the histograms of X-ray attenuation to discard voxels represented by a separate peak/tail outside normal distribution of the myocardium and the blood pool, respectively [13, 28, 29]. To allow visualization of stress perfusion defects, subendocardial attenuation was calculated across the inner 50% of the myocardial thickness and normalized by adjacent LV cavity attenuation for each node. All values were expressed in percent of the maximum value, and a median filter was used to smooth the color-encoded display.

Image fusion

Resting CTCA images were exported in DICOM format into Matlab to extract the coronary tree using previously described custom software [15]. The subendocardial stress perfusion data were mapped onto the endocardial surface and fused with the coronary arteries, resulting in a combined 3D display of the coronary anatomy and myocardial perfusion. The entire processing time was 15–20 min, once the data files are loaded. This display, with perfusion color-encoded onto the endocardial surface, was viewed from different angles (Video 1). This was done to determine the presence of a perfusion defect, defined as an area of non-uniform color distribution, in the territory underlying each artery, while taking into account the individual coronary anatomy by its direct visualization (Video 2).

Inter-technique comparisons

CTCA interpretation of coronary anatomy, performed on the resting images by an experienced reader, included the determination of presence, location and extent of stenosis in percent of luminal narrowing. Coronary arteries were then divided into three categories: (1) < 50% luminal narrowing and no clear perfusion defect, reflecting normal hemodynamics, (2) > 50% luminal narrowing and a visible perfusion defect, reflecting significant stenosis, and (3) either a

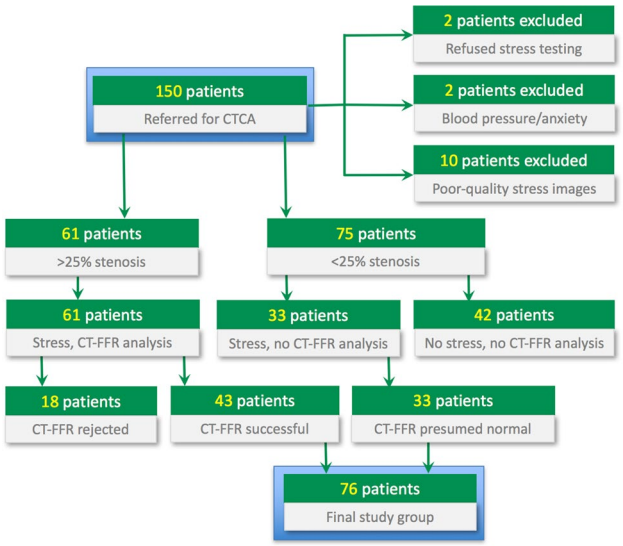

Fig. 2 Flowchart of patient enrollment through the formation of the final study group (see text for details)

perfusion defect without stenosis > 50% or stenosis > 50% without a perfusion defect, which were interpreted as insufficient evidence of hemodynamic impairment.

In patients with stenosis > 25% in ≥ 1 artery, CT-FFR analysis was performed from the resting CT datasets (HeartFlow, Redwood City, CA). This analysis included fluid dynamics based calculation of FFR for each coronary artery. FFR values was read approximately 1 cm distally to stenosis seen on CTCA. Calculated FFR values were used to categorize each coronary artery as either normal if FFR > 0.80, or as having hemodynamically significant stenosis if CT-FFR ≤ 0.80.

Outcomes

Composite outcomes that included death, myocardial infarction or revascularization were collected through chart review, Social Security Death Index search, and direct communication with patients/family and referring physicians.

Statistical analysis

To determine the level of agreement between the above two approaches, 2 × 2 contingency tables were created for each comparison and populated with numbers of arteries where both techniques indicated the presence or absence of significant disease, and those where they disagreed. These tables

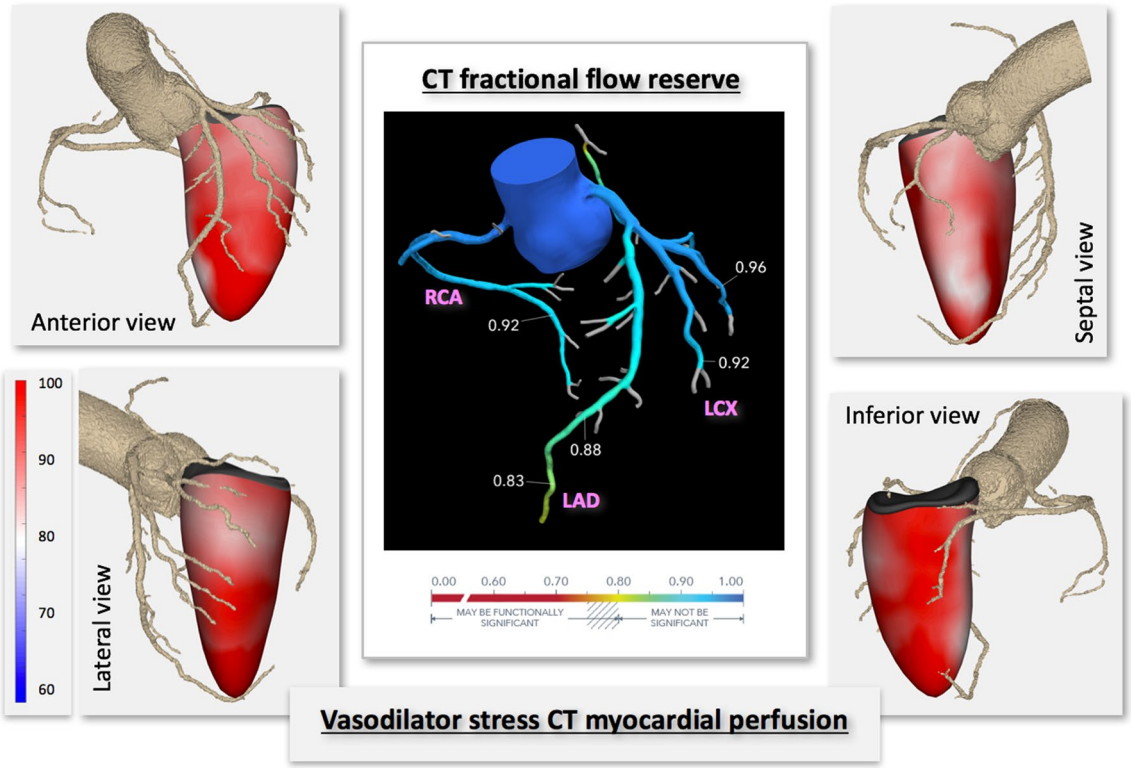

Fig. 3 Example of combined 3D display of myocardial perfusion during vasodilator stress and the coronary arteries obtained in a patient with no significant stenosis (left and right panels). The four snapshots depict the different views with fairly uniform subendocardial perfusion during vasodilator stress, reflected by the red hues. The snapshot of CT-FFR analysis (center) shows normal FFR in all three major coronary arteries, reflected by values > 0.80

were used to calculate the overall agreement (in percent of the total number of arteries), which was also assessed using kappa-statistics. The calculated kappa coefficients were judged as follows: 0–0.2 low, 0.2–0.4 moderate, 0.4–0.6 substantial, 0.6–0.8 good, and > 0.8 excellent.

Results

Of the 150 patients, two refused stress testing after signing informed consent, and two were not given regadenoson for safety concerns. Technical issues (e.g. infusion pump malfunction) and poor quality of stress CT images that precluded perfusion analysis (e.g. insufficient contrast due to incorrect timing of acquisition), resulted in exclusion of 10 additional patients. Figure 2 shows the scheme of patient enrollment through the formation of the final study group. Of the remaining 136 patients, 75 patients had either minimal stenosis with narrowing < 25% or no evidence of disease. Of these, 42 patients did not undergo vasodilator stress imaging to avoid unnecessary radiation, and were not included in the final analysis. The remaining 33/75 patients completed the imaging protocol to ensure a balanced sample of patients with and without disease. These 33 patients were not submitted for CT-FFR analysis, but were presumed to have normal FFR, based on the findings of no stenosis, and were included in the final analysis. The remaining 61 patients had stenosis with luminal narrowing > 25% and were submitted for CT-FFR analysis, but 18 of them (30%) were rejected due to motion artifacts, resulting in 43 patients with successful CT-FFR analysis. This resulted in a total of 76 patients, who comprised the final study group.

The combined 3D displays allowed visualization of subendocardial perfusion at peak stress in the territory of each artery. Figure 3 shows an example obtained in a patient with no significant stenosis, depicting fairly uniform normal (red) stress perfusion (left and right), consistent with normal CT-FFR > 0.80 in all three arteries (middle).

In contrast, Fig. 4 shows images from a patient who had a single-vessel disease with a 50–60% stenosis in the proximal left anterior descending (LAD) artery, resulting in a subendocardial SPD in the septum and the anteroseptal wall. Figure 5 shows the results of the CT-FFR analysis, depicting reduced FFR in this artery (top), as well as the results of image fusion (bottom), depicting an extensive perfusion defect in the LAD territory (blue), while the lateral and inferior walls show normal perfusion (red).

Figure 6 shows an example of images obtained in another patient with multivessel disease, with approximately 60% stenosis in both mid LAD and distal right coronary artery (RCA). Based on CT-FFR values ≤ 0.80, both lesions were hemodynamically significant. The fused 3D display showed a perfusion defect following the course of the LAD and extending to the apex (top, left and right), as well as

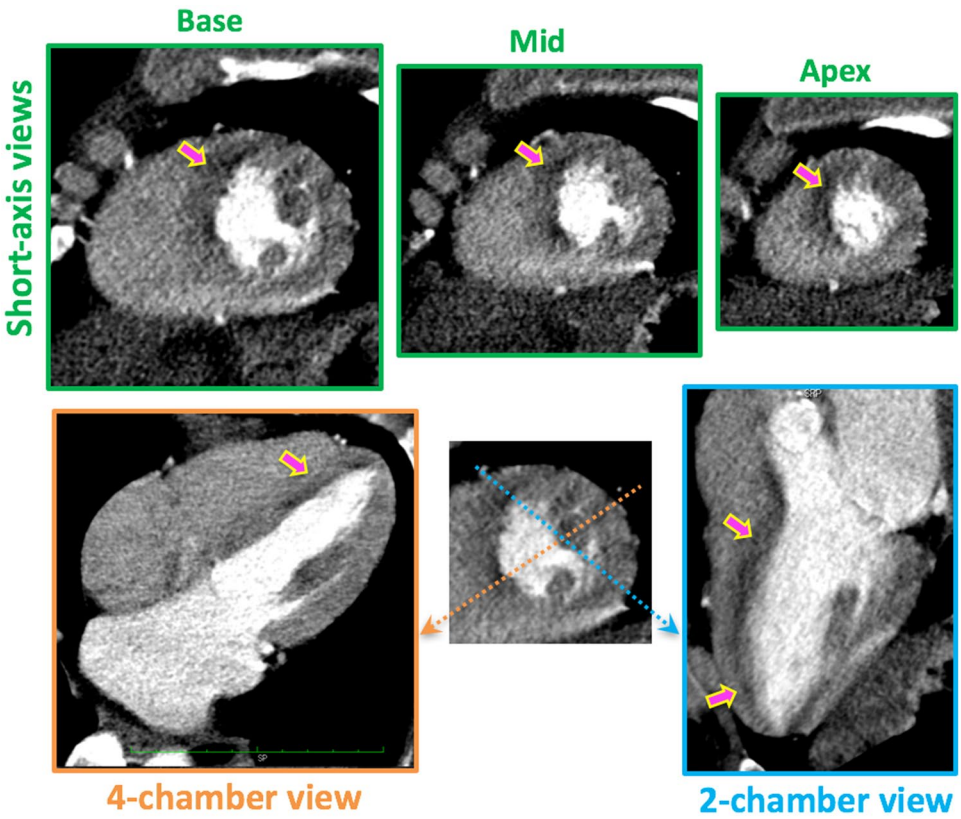

Fig. 4 Example of CT images obtained during vasodilator stress in a patient with an intermediate grade stenosis, resulting in 50–60% luminal narrowing. Subendocardial perfusion defect can be seen in the antero-septal and septal walls (arrows) in the different cross-sections of the heart

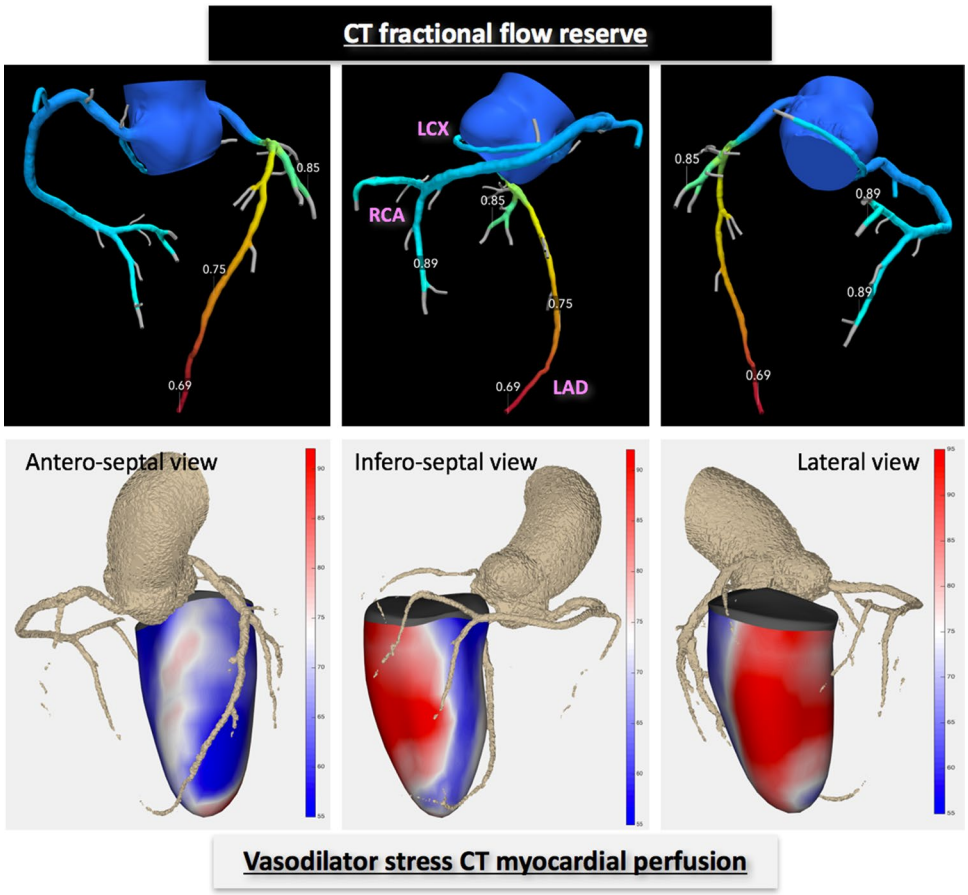

Fig. 5 Example of CT-FFR snapshots (top) and corresponding views of the combined 3D display of myocardial perfusion during vasodilator stress and the coronary arteries (bottom), obtained during vasodilator stress in a patient with an intermediate grade stenosis, resulting in 50–60% luminal narrowing in the proximal LAD. Reduced CT-FFR can be seen distal to the lesion (top), concomitant with a large perfusion abnormality encompassing the antero-septal and septal walls (bottom; blue hues)

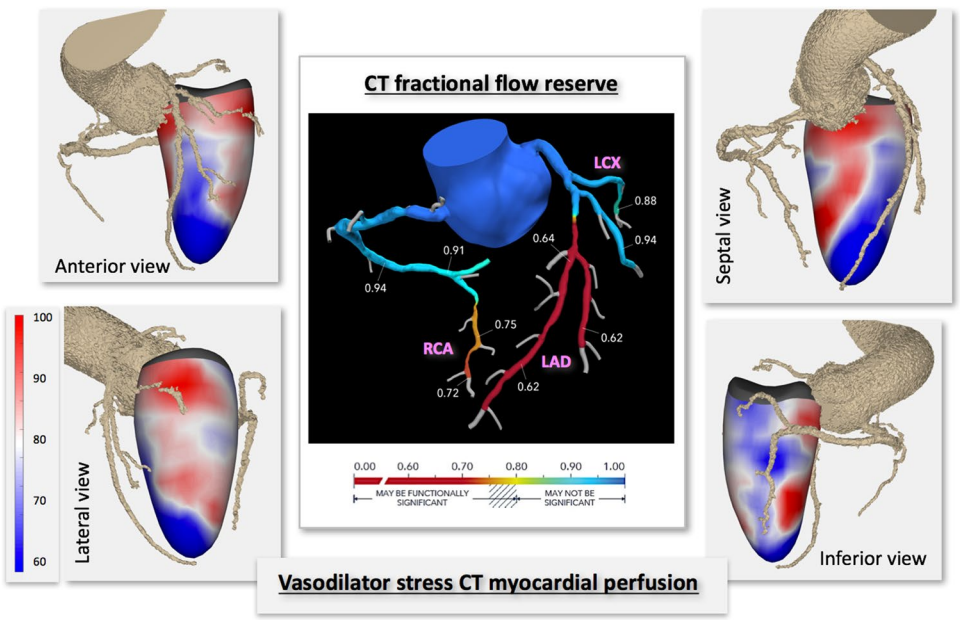

Fig. 6 Example of 3D display obtained in a patient with complex multivessel disease, with approximately 60% stenosis in the mid LAD and a similar lesion in the distal RCA, shown in the same format as in Fig. 3. Both lesions were determined to be significant by CT-FFR analysis, resulting in values < 0.80 (center). An extensive perfusion defect is seen in the anterior and antero-septal walls extending to the apex, supplied by the LAD artery (top left and right; blue hues), and another one in the inferior wall along the course of the RCA (bottom right), while perfusion in the lateral wall supplied by the stenosis-free LCX artery appears to be normal (bottom left; red hues)

abnormal perfusion in the inferior wall supplied by the RCA (bottom, right), while perfusion remained normal in the lateral wall supplied by the left circumflex (LCX) artery.

In the final study group of 76 patients, of the 228 coronary arteries (= 76 × 3), 4 arteries had stents, precluding CT-FFR analysis, and were excluded from analysis, allowing for

224 inter-technique comparisons. CTCA depicted stenosis > 70% in 13 arteries, stenosis between 50 and 70% in 24 arteries, stenosis < 50% in 63 arteries and 124 arteries were free of stenosis.

Reduced CT-FFR ≤ 0.80 was found in 41/224 arteries (18%), indicating hemodynamically significant stenosis in 29/76 patients (38%). In contrast, SPDs were noted in considerably more coronary territories: 85/224 arteries (37%), indicating significant disease in 56/76 patients (74%). Combining stress CTP with stenosis of > 50% on CTCA, resulted in considerably fewer abnormalities: 31/224 arteries (14%), indicating significant disease in 35/76 patients (46%).

Also of note, the prevalence of SPDs was considerably higher for arteries with CT-FFR ≤ 0.80 (33/41; 80%), compared to normal CT-FFR (52/183; 28%). Similarly, the combination of SPD with stenosis > 50% was more common in arteries with abnormal CT-FFR (24/41; 59%), compared to normal CT-FFR (7/183; 4%), with the difference being more pronounced than for SPDs alone.

Figure 7 shows the inter-technique agreement for stress perfusion fused with CTCA, and also for the combination with stenosis > 50% on CTCA, both against CT-FFR. The former comparison showed agreement in 73% of the arteries and a kappa-value of 0.368 (SE 0.060), indicating moderate agreement. The latter comparison incorporating stenosis showed agreement in 89% of the arteries and a higher kappa-value of 0.604 (SE 0.073), indicating good agreement.

The main source of disagreement that resulted in a relatively large number of SPDs that could not be explained by stenosis was streak artifacts caused by beam-hardening from highly attenuating in-plane structures. For example, patient shown in Fig. 8 had a large perfusion defect encompassing infero-septal, inferior and infero-lateral walls in the presence of normal RCA and LCX arteries (Fig. 8, left and right). Examination of the raw CT images revealed a large streak artifact (Fig. 8, middle, green arrows) caused by the spinal vertebrae, causing the false SPD.

On a patient-by-patient basis, 30/76 patients (39%) had hemodynamically significant stenosis based on abnormal CT-FFR in at least one artery, but only 7/76 patients (9%) reached the composite end-point of death (N = 1), myocardial infarction (N = 0) or revascularization (N = 6) over a follow-up period of 36 ± 25 months. Of the 30 patients with abnormal CT-FFR, 21 had an SPD in a territory of an artery with stenosis > 50%, and 9 had normal stress perfusion. Of the above 7 patients with adverse outcomes, 6 had abnormal CT-FFR and 6 had SPDs, with 2 patients showing discordant CT-FFR and CTP. Interestingly, of the 6 patients with

		SPD		Stenosis + SPD	
		Yes	No	Yes	No
CT-FFR	Abnormal (≤0.80)	33	8	24	17
	Normal (>0.80)	52	131	7	176
		kappa=0.368		kappa=0.604	

Fig. 7 Inter-technique agreement for stress perfusion defects (SPD) fused with CTCA, and also for the combination with stenosis > 50% on CTCA, both against CT-FFR, presented on a by-artery basis. See text for details

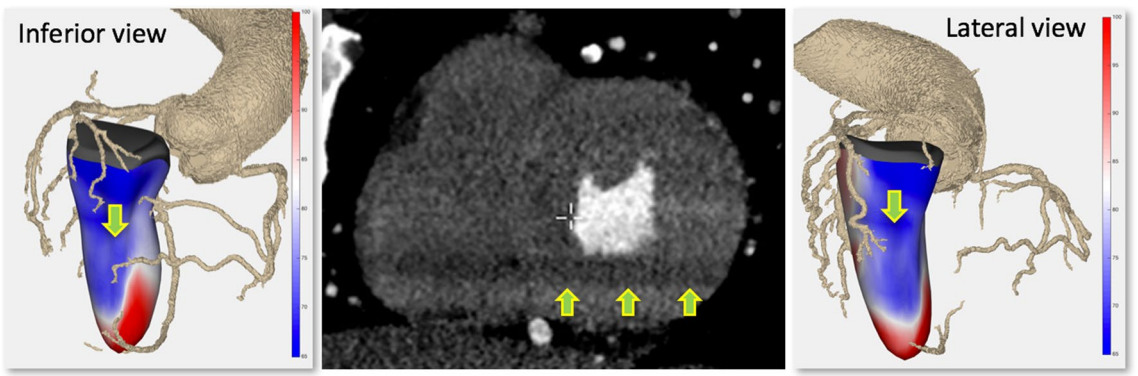

Fig. 8 Example of a combined 3D display depicting a large subendocardial stress perfusion defect covering infero-septal, inferior and inferolateral walls, in the presence of normal RCA and LCX arteries (arrows; left and right panels). Examination of the raw CT images of this patient revealed a large streak artifact caused by the spinal vertebrae (arrows; middle panel)

abnormal CT-FFR, 5 had a concomitant SPD (out of 21 patients with both abnormal CT-FFR and SPD, i.e. 24%), while only 1 patient had normal perfusion (out of 9 patients with abnormal CT-FFR but normal perfusion, i.e. 11%).

Discussion

While radionuclide myocardial perfusion imaging (MPI) during vasodilator stress is routinely used to elucidate the impact of stenosis seen on CTCA in patients with chest pain, it is an additional test associated with significant inconvenience to the patient, and additional radiation. Moreover, recent studies have suggested the diagnostic performance of nuclear MPI may be worse than previously thought [30]. Stress CTP imaging has been increasingly gaining recognition as an alternative to nuclear MPI [6, 9, 11, 14, 27, 31–37], and can be easily performed in patients undergoing CTCA with minimal additional radiation, in the same setting. However, it is often difficult to guarantee that an SPD is accurately attributed to stenosis in a specific coronary artery. This is because it requires one to mentally co-register perfusion information within the widely variable complex 3D coronary anatomy. This is particularly challenging in the setting of multi-vessel disease, when it is unclear which artery is responsible for the symptoms.

To overcome this limitation, we recently explored the feasibility of image fusion [38–45] of CTCA-derived coronary arteries and CTP maps, which was motivated by the thought that stress subendocardial perfusion displayed together with the coronary arteries could eliminate the need for mental reconciliation of the coronary anatomy and perfusion territories, and thereby facilitate the evaluation of hemodynamic impact of coronary stenosis, as a potential alternative to radionuclide MPI [15]. Our recent pilot study indicated that fusion of coronary arteries with perfusion maps may indeed depict the culprit artery and the impact of stenosis in its territory. However, this approach has not been compared to another technique aimed at the same goal, namely CT-FFR.

In the current study, we did not treat CT-FFR as a substitute for FFR measured during invasive coronary angiography. This is because of the growing evidence that CT-FFR has limitations resulting in imperfect specificity, especially in patients with intermediate grade stenosis [46]. Also, the feasibility of CT-FFR is limited in the presence of motion artifacts, which resulted in rejection of 18/61 (almost 30%) of the datasets submitted for analysis in our study. This higher than previously reported rate may be due to the specific equipment used, that might have been under-represented in previous studies. Thus, instead of treating CT-FFR as a surrogate "gold standard", our inter-technique comparisons were designed to simply determine the agreement between CTP and CT-FFR in the assessment of the hemodynamic impact of stenosis, which has not been studied thus far.

Our study showed in a relatively larger group of patients that stress perfusion abnormalities are considerably more common in the presence of stenosis with luminal narrowing > 50%, which results in reduced CT-FFR. Moreover, this study showed that subendocardial SPD appearing in the territory of an artery with stenosis > 50% indicates significant impact of disease, in reasonable agreement with CT-FFR data. The main source of discordance was dark streak-shaped beam hardening artifacts mimicking perfusion defects on 3D perfusion maps. It is also possible that some of the discordance between CTP and FFR may be due to microvascular disease [47]. Future studies are needed to determine whether abnormal CTP in the presence of normal CT-FFR is indeed associated with worse outcomes.

Interestingly, in our study, despite the relatively high incidence of abnormal CT-FFR (30 out of 76 patients), a considerably smaller number of patients (N = 7) experienced adverse outcomes over the 3-year follow-up period. This finding indicates that perhaps the 0.80 cutoff value may be too high when outcomes are considered, and that the majority of patients with abnormal CT-FFR, defined by this cutoff, may not experience adverse events over a relatively long period of time without intervention. Another interesting and potentially clinically useful finding is that in the presence of abnormal CT-FFR, the incidence of SPDs was more than twice as high as that of normal CTP (24 vs. 11%), and most patients who ultimately experienced poor outcomes had both abnormal CT-FFR and SPD (5/7). This suggests that when abnormal CT-FFR is detected, adding a vasodilator stress CT with perfusion analysis may identify patients who are less likely to require revascularization.

One potential limitation of our approach is that the quality of cardiac CT images depends on the patient's body mass. Accordingly, the feasibility of our approach, which is based on fusion of CT-derived images, is limited in obese patients.

The main limitation of quantitative analysis of myocardial perfusion from CT images is that it is prone to artifacts caused by beam hardening, which mimic perfusion defects. To avoid misdiagnosis, it is important to review the raw images when quantitative analysis suggests abnormal perfusion. The presence of a streak artifact over the myocardium which extends to other structures irrespective of cardiac anatomy (Fig. 8) should rule out a true perfusion defect. Another strategy, to reduce the number of false positive perfusion defects, which proved effective, was the use of a combination of SPD and stenosis > 50% on CTCA, rather than SPD alone, as an indicator of hemodynamically significant stenosis. This is because of the low likelihood of an SPD without underlying stenosis with ≥ 50% luminal narrowing, based on well-established evidence that stenosis

of lower degree is unlikely to have hemodynamic/functional impact. Nevertheless, we included in our report the results of the comparisons of SPDs alone against CT-FFR (Fig. 7), in order to be able to appreciate the improvement in accuracy that the use of combined criteria provided.

The main limitation of our study was that we did not use invasive FFR, as a reference standard for hemodynamic impact of stenosis. This is because this approach was impractical as it would inevitably severely limit the number of patients we could evaluate and would bias the study population by excluding those not considered to be at high enough risk to justify a referral for invasive angiography. A plausible alternative was the non-invasive fluid dynamics based CT-FFR analysis[17], which could theoretically be performed in every study patient. Ultimately, we decided to limit CT-FFR analysis to patients with evidence of $\geq 25\%$ luminal narrowing, since the likelihood of abnormal FFR is extremely low in the absence of at least minimally obstructive coronary disease. Another consideration for this study design was that it did not make sense to perform expensive CT-FFR analysis in patients with normal coronaries.

Another limitation of our study is the relatively small number of outcomes, limiting our ability to generalize our findings related to prognostic value of these tests. However, with the low rate of events in this patient population, a sample of thousands would need to be prospectively studied to alleviate this concern.

Finally, one might question our choice to detect perfusion abnormalities qualitatively by visual assessment of the color-coded perfusion maps, rather than by quantitative analysis. In our recent pilot study, our attempts to define them quantitatively resulted in missing many of the visible abnormalities because of the large size and the location of the segments relative to the size and the location of the defects [15]. One may appreciate in the example shown in Fig. 6 how perfusion defects follow the course of the culprit artery, which cannot be respected by dividing the ventricle into regularly shaped segments [15]. Accordingly, we felt that qualitative visual assessment of the high-resolution parametric perfusion images was best to detect these abnormalities.

In summary, fusion of CTCA and normalized subendocardial X-ray attenuation allows direct visualization of each coronary artery and stress CTP in its territory without the need to mentally co-register them within the complex 3D cardiac anatomy. In this study, stress perfusion abnormalities were considerably more common in the territories of arteries with stenosis resulting in reduced CT-FFR in patients with chest pain. In addition, our approach for determination of hemodynamic impact of stenosis showed good agreement with CT-FFR determination of the significance of stenosis. Our outcomes data suggests that adding a vasodilator stress CT with perfusion analysis may help with further risk stratification in patients with abnormal CT-FFR. This methodology may prove as a useful alternative to radionuclide perfusion imaging, with the advantages of simplicity and convenience due to its single-test nature, entailing considerable cost savings and reduced radiation exposure to the patient.

Acknowledgements This study was funded by a research grant from Astellas Pharma Global Development (Grant No. REGA-13H05). Four of the coauthors (AN, AM, AS and KK) were supported by the NIH T32 Cardiovascular Sciences Training Grant (5T32HL7381). HeartFlow provided analyses for free. Dr. Patel and Dr. Lang have research support from Philips for other projects.

Compliance with ethical standards

Conflict of interest The authors declare that they have no conflict of interest.

Ethical approval All procedures performed in studies involving human participants were in accordance with the ethical standards of the institutional and/or national research committee and with the 1964 Helsinki declaration and its later amendments or comparable ethical standards.

Informed consent The study was approved by the Institutional Review Board with a waiver of consent.

References

1. Garcia MJ, Lessick J, Hoffmann MH, Investigators CS (2006) Accuracy of 16-row multidetector computed tomography for the assessment of coronary artery stenosis. JAMA 296:403–411
2. Miller JM, Rochitte CE, Dewey M et al (2008) Diagnostic performance of coronary angiography by 64-row CT. N Engl J Med 359:2324–2336
3. Schroeder S, Achenbach S, Bengel F et al (2008) Cardiac computed tomography: indications, applications, limitations, and training requirements: report of a Writing Group deployed by the Working Group Nuclear Cardiology and Cardiac CT of the European Society of Cardiology and the European Council of Nuclear Cardiology. Eur Heart J 29:531–556
4. Pijls NH, De Bruyne B, Peels K et al (1996) Measurement of fractional flow reserve to assess the functional severity of coronary–artery stenoses. N Engl J Med 334:1703–1708
5. Tonino PA, Fearon WF, De Bruyne B et al (2010) Angiographic versus functional severity of coronary artery stenoses in the FAME study fractional flow reserve versus angiography in multivessel evaluation. J Am Coll Cardiol 55:2816–2821
6. George RT, Silva C, Cordeiro MA et al (2006) Multidetector computed tomography myocardial perfusion imaging during adenosine stress. J Am Coll Cardiol 48:153–160
7. Ko BS, Cameron JD, Defrance T, Seneviratne SK (2011) CT stress myocardial perfusion imaging using multidetector CT—a review. J Cardiovasc Comput Tomogr 5:345–356
8. Techasith T, Cury RC (2011) Stress myocardial CT perfusion: an update and future perspective. JACC Cardiovasc Imaging 4:905–916
9. Blankstein R, Shturman LD, Rogers IS et al (2009) Adenosine-induced stress myocardial perfusion imaging using dual-source cardiac computed tomography. J Am Coll Cardiol 54:1072–1084

10. Bastarrika G, Ramos-Duran L, Rosenblum MA, Kang DK, Rowe GW, Schoepf UJ (2010) Adenosine-stress dynamic myocardial CT perfusion imaging: initial clinical experience. Invest Radiol 45:306–313
11. Rocha-Filho JA, Blankstein R, Shturman LD et al (2010) Incremental value of adenosine-induced stress myocardial perfusion imaging with dual-source CT at cardiac CT angiography. Radiology 254:410–419
12. Bettencourt N, Rocha J, Ferreira N et al (2011) Incremental value of an integrated adenosine stress-rest MDCT perfusion protocol for detection of obstructive coronary artery disease. J Cardiovasc Comput Tomogr 5:392–405
13. Patel AR, Lodato JA, Chandra S et al (2011) Detection of myocardial perfusion abnormalities using ultra-low radiation dose regadenoson stress multidetector computed tomography. J Cardiovasc Comput Tomogr 5:247–254
14. Ko BS, Cameron JD, Meredith IT et al (2012) Computed tomography stress myocardial perfusion imaging in patients considered for revascularization: a comparison with fractional flow reserve. Eur Heart J 33:67–77
15. Maffessanti F, Patel AR, Patel MB et al (2017) Non-invasive assessment of the haemodynamic significance of coronary stenosis using fusion of cardiac computed tomography and 3D echocardiography. Eur Heart J Cardiovasc Imaging 18:670–680
16. Koo BK, Erglis A, Doh JH et al (2011) Diagnosis of ischemia-causing coronary stenoses by noninvasive fractional flow reserve computed from coronary computed tomographic angiograms. Results from the prospective multicenter DISCOVER-FLOW (diagnosis of ischemia-causing stenoses obtained via noninvasive fractional flow reserve) study. J Am Coll Cardiol 58:1989–1997
17. Min JK, Leipsic J, Pencina MJ et al (2012) Diagnostic accuracy of fractional flow reserve from anatomic CT angiography. JAMA 308:1237–1245
18. Nakazato R, Park HB, Berman DS et al (2013) Noninvasive fractional flow reserve derived from computed tomography angiography for coronary lesions of intermediate stenosis severity: results from the DeFACTO study. Circ Cardiovasc Imaging 6:881–889
19. Renker M, Schoepf UJ, Wang R et al (2014) Comparison of diagnostic value of a novel noninvasive coronary computed tomography angiography method versus standard coronary angiography for assessing fractional flow reserve. Am J Cardiol 114:1303–1308
20. Voros S, Rinehart S, Vazquez-Figueroa JG et al (2014) Prospective, head-to-head comparison of quantitative coronary angiography, quantitative computed tomography angiography, and intravascular ultrasound for the prediction of hemodynamic significance in intermediate and severe lesions, using fractional flow reserve as reference standard (from the ATLANTA I and II Study). Am J Cardiol 113:23–29
21. Baumann S, Renker M, Hetjens S et al (2016) Comparison of coronary computed tomography angiography-derived vs invasive fractional flow reserve assessment: meta-analysis with subgroup evaluation of intermediate stenosis. Acad Radiol 23:1402–1411
22. Gaur S, Ovrehus KA, Dey D et al (2016) Coronary plaque quantification and fractional flow reserve by coronary computed tomography angiography identify ischaemia-causing lesions. Eur Heart J 37:1220–1227
23. Kawaji T, Shiomi H, Morishita H et al (2017) Feasibility and diagnostic performance of fractional flow reserve measurement derived from coronary computed tomography angiography in real clinical practice. Int J Cardiovasc Imaging 33:271–281
24. Rabbat MG, Berman DS, Kern M et al (2017) Interpreting results of coronary computed tomography angiography-derived fractional flow reserve in clinical practice. J Cardiovasc Comput Tomogr 11:383–3388
25. Nieman K, Shapiro MD, Ferencik M et al (2008) Reperfused myocardial infarction: contrast-enhanced 64-Section CT in comparison to MR imaging. Radiology 247:49–56
26. So A, Hsieh J, Li JY, Hadway J, Kong HF, Lee TY (2012) Quantitative myocardial perfusion measurement using CT perfusion: a validation study in a porcine model of reperfused acute myocardial infarction. Int J Cardiovasc Imaging 28:1237–1248
27. Nasis A, Ko BS, Leung MC et al (2013) Diagnostic accuracy of combined coronary angiography and adenosine stress myocardial perfusion imaging using 320-detector computed tomography: pilot study. Eur Radiol 23:1812–1821
28. Kachenoura N, Veronesi F, Lodato JA et al (2010) Volumetric quantification of myocardial perfusion using analysis of multidetector computed tomography 3D datasets: comparison with nuclear perfusion imaging. Eur Radiol 20:337–347
29. Mor-Avi V, Lodato JA, Kachenoura N et al (2012) Quantitative three-dimensional evaluation of myocardial perfusion during regadenoson stress using multidetector computed tomography. J Comput Assist Tomogr 36:443–449
30. Takx RA, Blomberg BA, El Aidi H et al (2015) Diagnostic accuracy of stress myocardial perfusion imaging compared to invasive coronary angiography with fractional flow reserve meta-analysis. Circ Cardiovasc Imaging 8:e002666
31. Cury RC, Magalhaes TA, Borges AC et al (2010) Dipyridamole stress and rest myocardial perfusion by 64-detector row computed tomography in patients with suspected coronary artery disease. Am J Cardiol 106:310–315
32. Bamberg F, Klotz E, Flohr T et al (2010) Dynamic myocardial stress perfusion imaging using fast dual-source CT with alternating table positions: initial experience. Eur Radiol 20:1168–1173
33. Okada DR, Ghoshhajra BB, Blankstein R et al (2010) Direct comparison of rest and adenosine stress myocardial perfusion CT with rest and stress SPECT. J Nucl Cardiol 17:27–37
34. Bettencourt N, Chiribiri A, Schuster A et al (2013) Direct comparison of cardiac magnetic resonance and multidetector computed tomography stress-rest perfusion imaging for detection of coronary artery disease. J Am Coll Cardiol 61:1099–1107
35. George RT, Arbab-Zadeh A, Cerci RJ et al (2011) Diagnostic performance of combined noninvasive coronary angiography and myocardial perfusion imaging using 320-MDCT: the CT angiography and perfusion methods of the CORE320 multicenter multinational diagnostic study. AJR Am J Roentgenol 197:829–837
36. Ko BS, Cameron JD, Leung M et al (2012) Combined CT coronary angiography and stress myocardial perfusion imaging for hemodynamically significant stenoses in patients with suspected coronary artery disease: a comparison with fractional flow reserve. JACC Cardiovasc Imaging 5:1097–1111
37. Vavere AL, Simon GG, George RT et al (2011) Diagnostic performance of combined noninvasive coronary angiography and myocardial perfusion imaging using 320 row detector computed tomography: design and implementation of the CORE320 multicenter, multinational diagnostic study. J Cardiovasc Comput Tomogr 5:370–381
38. Gaemperli O, Schepis T, Kalff V et al (2007) Validation of a new cardiac image fusion software for three-dimensional integration of myocardial perfusion SPECT and stand-alone 64-slice CT angiography. Eur J Nucl Med Mol Imaging 34:1097–1106
39. Nakaura T, Utsunomiya D, Shiraishi S et al (2005) Images in cardiovascular medicine. Fusion imaging between myocardial perfusion single photon emission computed tomography and cardiac computed tomography. Circulation 112:e47–e48
40. Tian J, Smith MF, Jeudy J, Dickfeld T (2009) Multimodality fusion imaging using delayed-enhanced cardiac magnetic resonance imaging, computed tomography, positron emission

tomography, and real-time intracardiac echocardiography to guide ventricular tachycardia ablation in implantable cardioverter-defibrillator patients. Heart Rhythm 6:825–828
41. Stolzmann P, Alkadhi H, Scheffel H et al (2010) Image fusion of coronary CT angiography and cardiac perfusion MRI: a pilot study. Eur Radiol 20:1174–1179
42. Yoshikai M, Ikeda K, Itoh M, Ueno Y (2009) Cardiac fusion image from myocardial perfusion scintigraphy and 64-slice computed tomography before and after coronary artery bypass grafting. Eur J Cardiothorac Surg 35:1078
43. Donati OF, Alkadhi H, Scheffel H et al (2011) 3D fusion of functional cardiac magnetic resonance imaging and computed tomography coronary angiography: accuracy and added clinical value. Invest Radiol 46:331–340
44. Duckett SG, Ginks M, Shetty AK et al (2011) Realtime fusion of cardiac magnetic resonance imaging and computed tomography venography with X-ray fluoroscopy to aid cardiac resynchronisation therapy implantation in patients with persistent left superior vena cava. Europace 13:285–286
45. Manka R, Kuhn FP, Kuest SM, Gaemperli O, Kozerke S, Kaufmann PA (2011) Hybrid cardiac magnetic resonance/computed tomographic imaging: first fusion of three-dimensional magnetic resonance perfusion and low-dose coronary computed tomographic angiography. Eur Heart J 32:2625
46. Cook CM, Petraco R, Shun-Shin MJ et al (2017) Diagnostic accuracy of computed tomography-derived fractional flow reserve: a systematic review. JAMA Cardiol 2:803–810
47. Zorach B, Shaw PW, Bourque J et al (2018) Quantitative cardiovascular magnetic resonance perfusion imaging identifies reduced flow reserve in microvascular coronary artery disease. J Cardiovasc Magn Reson 20:14